Single electron quantum dot in a spatially periodic magnetic field

D. Buchholz,[1] P. S. Drouvelis,[1] and P. Schmelcher[1,2]

[1]*Theoretische Chemie, Institut für Physikalische Chemie, Universität Heidelberg, Im Neuenheimer Feld 229,*
69120 Heidelberg, Germany
[2]*Physikalisches Institut, Universität Heidelberg, Philosophenweg 12, 69120 Heidelberg, Germany*

A harmonic single electron quantum dot in a spatially periodic magnetic field is investigated. The energy spectrum, magnetization, probability, and current density are studied for varying parameters (i.e., amplitude, wavelength, and phase) of the periodic magnetic field. For wavelengths comparable to the oscillator length of the dot, we observe a rich spectral behavior. For higher field amplitudes and depending on the phase of the field, avoided and exact level crossings dominate the spectrum and quasidegenerate low lying states occur systematically. We employ a simple model for the interpretation of the quasidegeneracies and their impact on the probability and current densities. The latter are very sensitive with respect to the phase of the magnetic field. For wavelengths being small compared to the oscillator length, the impact of the field is very minor, thus the obtained spectrum is approximately that of a pure harmonic oscillator. For large values of k the eigenfunctions take up a spatially varying phase and the magnitude of the probability current decreases slowly with increasing k. Different from the dot in a homogeneous magnetic field, the magnetization, as a function of the field amplitude, has a minimum, depending on the phase and wavelength of the field.

I. INTRODUCTION

Artificial semiconductor nanostructures especially their electronic properties have been investigated intensively during the last decades. Conduction band electrons of a semiconductor can be confined to a so-called quantum well by sandwiching a thin flat layer of a certain semiconductor between two layers of another semiconductor, which possesses a higher conduction band energy. The electrons bound inside the quantum well consisting of only a few crystalline monolayers form a so-called two-dimensional electron gas (2DEG). Their motion is restricted to the plane perpendicular to the quantum well and the excitations in the direction of the well are strongly quantized and energetically well-separated.[1,2] These quasi-two-dimensional systems exhibit unusual properties and have nowadays many applications in electronics and/or optoelectronics. By etching structures on the basis of a quantum well or applying additional electrostatic potentials, the motion of the electrons can be constrained further to one or zero dimensions. Respective objects are the so-called quantum wires[3] and quantum dots. Because of the fact that the shape of the dot, i.e., the confining potential, and the number of confined electrons can be controlled very well in the experiment, quantum dots provide a realization of few body quantum problems. On the other hand it can be expected that the theoretical modeling of quantum dots will reveal general properties of nanostructures being of interest for the design of microelectronic devices. The energy spectra of quantum dots can, for example, be measured by single-electron transport spectroscopy.[4,5] Many properties of the obtained spectra can be explained theoretically if the confining potential of the quantum dot is approximated by a parabolic well. General overviews on the electronic properties of quantum dots are given in the book of Hawrylack *et al.*[6] and the reviews of Kouwenhoven *et al.*[4] and Reimann *et al.*,[7] for example.

The combination of microstructures and external magnetic fields has provided rich new physics. The integer quantum Hall effect[8] and the fractional quantum Hall effect[9] are effects of a homogeneous magnetic field on a 2DEG. Physics of 2DEGs are in general well understood, see, e.g., the review of Beenakker[10] and references therein. The influence of a homogeneous field upon a quantum dot has been investigated in detail in the past. The solutions of the Schrödinger equation for a single charged particle inside an isotropic parabolic potential and a magnetic field are the Fock-Darwin states.[11,12] For an anisotropic charged harmonic oscillator (HO) inside a magnetic field there still exist analytic solutions of the Schrödinger equation.[13] Further on analytical solutions are known for two electrons inside an isotropic harmonic confinement and a homogeneous magnetic field, for particular configurations.[14,15] For more than one electron and an anisotropic confinement, the Schrödinger equation in general cannot be solved analytically. Numerical studies predict an influence of the dot's shape on the spectrum and thermodynamic properties like magnetization, see, for example, Refs. 16–18 and references therein. The effective Landé g-factor in a 2DEG can be tuned by applying a gate voltage perpendicular to the 2DEG.[19] In particular for a $Al_xGa_{1-x}As$ quantum well with gradually varying Al concentration along the z-direction a zero g-factor can be achieved.[20]

In addition to the scenario of homogeneous fields, a wide range of investigations with respect to spatially varying magnetic fields have been performed. In this respect 2DEGs have been exposed to magnetic steps, barriers, and wells.[21,22] Their electronic structure reveals bound states which lead to wave-vector dependent tunneling.[23] Alternatively, a magnetic field gradient imposed on a 2DEG can lead to unique magnetic edge states on the magnetic domain boundaries.[24,25] The effects of these states have also been identified in magnetotransport investigations through quantum wires, in which

the gradient is applied in the transversal direction.[26–28] Experimentally, rapid progress in microstructuring techniques has made possible the preparation of hybrid semiconductor/ ferromagnetic nanostructures in which the electronic motion sustains a spatially dependent inhomogeneous magnetic environment on the mesoscopic scale. Local magnetic field gradients have been applied experimentally on 2DEGs[29,30] giving rise to unique magnetotransport properties.

In a similar fashion spatially periodic magnetic fields can be experimentally prepared, if we depose, for example, an array of ferromagnetic gratings above a 2DEG. Particular interesting magnetotransport properties arise as a result of the commensurability between the electronic cyclotron radius and the period of the magnetic modulation. Hence, magnetic commensurability oscillations, the so-called Weiss oscillations, or giant magnetoresistances have been identified experimentally[31–35] in 1D magnetic superlattices created by arrays of ferromagnetic stripes. These results have been predicted by quasiclassical[36] and quantum mechanical[37–40] calculations. The role of electron-electron interactions in the resistivity of 2DEGs has also been investigated, both experimentally[41–43] and theoretically.[44] Two-dimensional periodic magnetic modulation can be formed as well, if we depose, e.g., ferromagnetic dots above 2DEGs.[45] Classically, the magnetic field modulation introduces a controlled transition from regular to mixed phase space[46] and ballistic high velocity modes of electrons[47] explain the observed peaks in the magnetoresistivity of an array of magnetic antidots.[48,49] Additionally to the above-mentioned investigations in 2DEGs, calculations of quantum transport through quantum wires under periodic magnetic fields have shown the formation of dips and minigaps in the magnetoconductance.[50,51]

These results in general naturally raise the question what happens if an electron confined in all spatial dimensions is exposed to a spatially periodic magnetic field. Yet there have not been studies of electrons in quantum dots, for which the wavelength is of the same order of magnitude as the length scale of the dot. This is mainly due to the reason that strong static magnetic fields with wavelengths below 1 μm are difficult to prepare experimentally. However, modern techniques of microstructuring and the possibility to prepare relatively large quantum dots, i.e., with diameter $\sim$1 μm, by electrostatic confinement make experiments with dots in the presence of periodic magnetic fields possible.

In this article we investigate the eigenenergies and eigenstates of a single, spin-less charged particle, confined in a two-dimensional isotropic dot exposed to a sinusoidally varying magnetic field. In Sec. II we derive the model for our quantum dot, and formulate our Hamiltonian as well. The method for the numerical solution of the corresponding Schrödinger equation is discussed in Sec. III. Complementary to this section, we discuss some details of our numerical procedure in two appendices for the interested reader. In Sec. IV we present and interpret the electronic structure of the dot. We further relate it to some experimentally measurable quantities such as the electrochemical potentials and the magnetization. Finally, probability and current densities complete our discussion. Section V contains the conclusions.
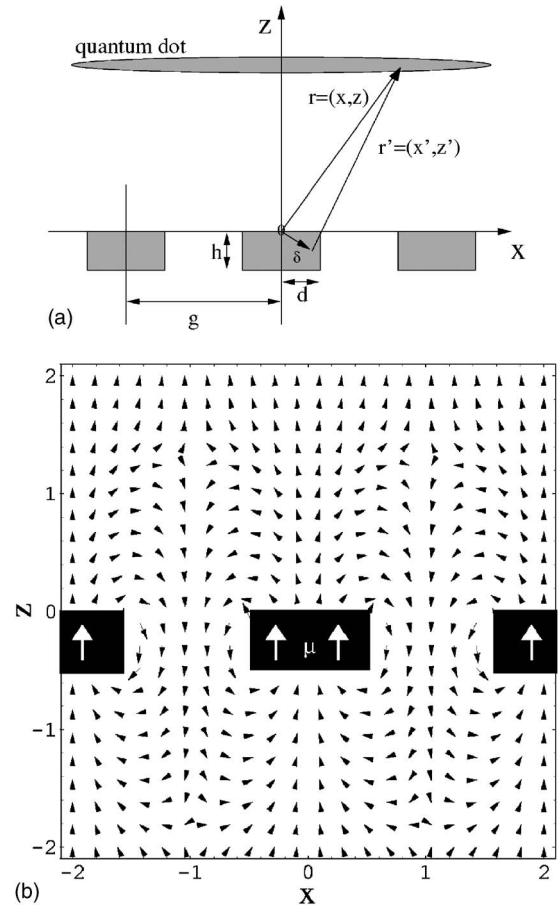

FIG. 1. Setup of the dot and magnetic field. (a) Section along the xz-plane. The grating is assumed to be translationally symmetric in the y-direction. (b) Vector-plot of the field in the xz-plane resulting from the example setup with magnetization directed along the z-axis.

II. MODEL OF THE QUANTUM DOT

A. Inhomogeneous magnetic fields on the nanometer scale

Inhomogeneous magnetic field configurations inside a semiconductor can be prepared as follows: A thin layer of ferromagnetic material is deposed on the surface of the semiconductor, using chemical vapor deposition or molecular beam epitaxy. Afterwards parts of the ferromagnetic layer are removed by etching. Exposing the remaining structure to an external homogeneous magnetic field will magnetize the ferromagnetic material, the resulting magnetic field varies on the length scale of the ferromagnetic structures. This technique has commonly been used in experiments with two-dimensional electron gases.[31–33,35,38,41,43] We now provide a calculation of the magnetic field $\vec{B}(x,y,z)$ generated by a grating of ferromagnetic bars with constant magnetization $\vec{\mu}$. The setup is shown in Fig. 1. The bars shall be infinitely long in the y-direction and the y-component μ_y of the magnetization is assumed to be zero due to the preparation of the system. It has experimentally been shown that a magnetization of thin ferromagnetic films in the out-of-plane direction can be achieved using a proper combination of, e.g., Fe and Ni layers on a GaAs substrate.[52] Therefore the y-component

of the magnetic field is also zero: $B_y(x,y,z)=0$. Here it is assumed that the semiconductor is not magnetizable. In this case, the field of a single bar extended from $x=-d$ to $x=d$ and $z=-h$ to $z=0$ is given by

$$\vec{B}(x,z) = \frac{\mu_0}{4\pi}\int_z^{z+h}dz'\int_{-\infty}^{\infty}dy'\int_{x-d}^{x+d}dx'\left(\frac{3\vec{r}'(\vec{r}'\vec{\mu})}{r'^5}-\frac{\vec{\mu}}{r'^3}\right).$$

$$(1)$$

Using the linearity with respect to $\vec{\mu}$ yields for the components:

$$B_x(x,z) = \frac{\mu_0}{4\pi}[\mu_x B_x^x(x,z) + \mu_z B_x^z(x,z)], \quad (2)$$

$$B_z(x,z) = \frac{\mu_0}{4\pi}[\mu_x B_z^x(x,z) + \mu_z B_z^z(x,z)], \quad (3)$$

with the dimensionless functions

$$B_x^x(x,z) = -B_z^z(x,z) = 2\arctan\left(\frac{z'}{x'}\right)\Big|_{x'=x-d}^{x'=x+d}\Big|_{z'=z+h}^{z'=z}, \quad (4)$$

$$B_x^z(x,z) = B_z^x(x,z) = \log\ (x'^2+z'^2)\Big|_{x'=x-d}^{x'=x+d}\Big|_{z'=z+h}^{z'=z}. \quad (5)$$

The lengths can be scaled to be dimensionless because the resulting field depends only on the ratios of the geometric parameters.

The field of the grating is then given by $\vec{B}(x,z)=\Sigma_{n=-\infty}^{\infty}\vec{B}(x+ng,z)$, where g is the separation of the centers of two neighboring bars. We have evaluated this sum numerically for a finite number of bars. To be specific we have chosen a grating consisting of 21 bars with the geometric parameters $d=0.5$, $h=0.5$, and $g=2$. When setting up the Hamiltonian, we will see that for our investigations exclusively the z-component of the field at the location of the quantum dot is of interest, i.e., $B_z(x,z)$ for small values of $|x|$ and constant z.

In Fig. 2 $B_z(x,z=0.5)$ is shown. Increasing the number of bars does not significantly change the field near $x=0$. For the chosen distance from the grating plane, a sinusoidally modulated field is a very good approximation to the calculated field modulation. If the distance z from the grating is much smaller, the magnetic field deviates severely from the sinusoidal shape. For a distance $z\approx\frac{g}{4}$ from the grating plane, the z-component of the magnetic field can approximately be described by $B_z(x)=B\cos(kx+\varphi)$, where $k=\frac{2\pi}{g}$. In this respect for an experimental setup with $g=400$ nm, the distance of the dot from the grating plane should be about 100 nm and its diameter has to be of the order of g, to obtain several oscillations of the field within the dot. The phase of the magnetic field can be changed by altering the direction of the bars' magnetization.

B. Hamiltonian and symmetries

In the following we present the model Hamiltonian for our system. For the dot confinement we choose a rotationally
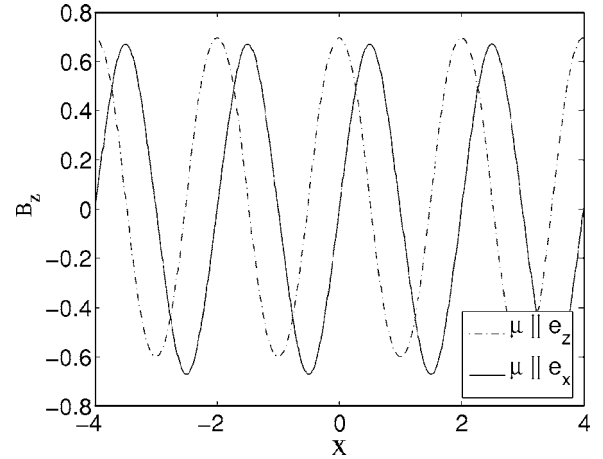

FIG. 2. z-component of the magnetic field generated by a grating, consisting of 21 bars with magnetization $\mu=\frac{4\pi}{\mu_0}$. The dimensions are $d=0.5$, $h=0.5$, and $g=2$ in arbitrary units. The solid line is the field strength for magnetization in the x-direction and the dash-dotted line for magnetization in the z-direction. The distance from the plane of the grating is $z=0.5$.

symmetric parabolic potential $V(x,y)=\frac{m\omega_0^2}{4}(x^2+y^2)$ within the plane of the dot. An additional z-dependent potential $V(z)$ is assumed providing a significantly stronger confinement, such that only the ground state in the z-direction will be occupied and a projection of the Hamiltonian is possible, thereby providing a 2D working Hamiltonian. Setting up the Hamiltonian for the general magnetic field derived in the previous section, it turns out that the x- and y-components of the magnetic field contribute to the Hamiltonian only via the corresponding spin-terms and via terms containing the factors z or z^2. Due to the strong confinement, the terms proportional to z or z^2 can be neglected. We focus here on the kinetic effects imposed by the periodic magnetic field and neglect the spin contribution which is motivated by the fact that the g-factor can be adjusted experimentally.[20] The expected effects of the spin are shortly discussed at the end of Sec. IV B. Only the z-component of the magnetic field then contributes to the kinetic terms within the full Schrödinger equation. The magnetic field reads $\vec{B}=[0,0,B_h+B\cos(kx+\varphi)]$. For reasons of generality and for the later on calculation of the magnetization of the dot in the presence of a periodic magnetic field we have taken into account a homogeneous magnetic field component B_h. Hence the Hamiltonian takes on the appearance $H=\frac{1}{2m^*}(\vec{p}-e\vec{A})^2+V(x,y)$. For the vector potential we use the gauge $\vec{A}=(-y[B_h+B\cos(kx+\varphi)],0,0)$, yielding the 2D working Hamiltonian

$$H = \frac{1}{2m^*}\{p_x^2+p_y^2+2e[B_h+B\cos(kx+\varphi)]yp_x$$

$$+i\hbar ekB\sin(kx+\varphi)y+e^2[B_h+B\cos(kx+\varphi)]^2y^2\}$$

$$+\frac{m^*\omega_0^2}{4}(x^2+y^2). \quad (6)$$

In the following we discuss the symmetries of H. First we employ a canonical transformation to introduce natural units
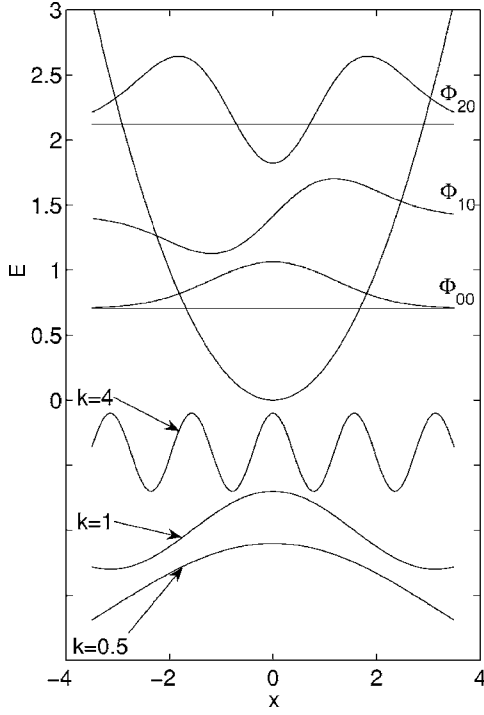
FIG. 3. Intersection of the potential $V(x, y=0)=\frac{x^2}{4}$, the HO eigenfunctions Φ_{00}, Φ_{10}, Φ_{20} each one shifted by its eigenenergy and the functions $\cos(0.5x)$, $\cos(x)$, and $\cos(4x)$. The effect of the periodic magnetic field is most pronounced when only about a half wavelength of the field fits inside the quantum dot.

for the quantum dot. For $\gamma \neq 0$, the Hamiltonian fulfills the following scaling relation:

$$H(\gamma\omega_0, \gamma B_h, \gamma B, \sqrt{\gamma}k\varphi; x, y) = \gamma H(\omega_0, B_h, B, k, \varphi; \sqrt{\gamma}x, \sqrt{\gamma}y).$$

(7)

The right-hand side of this equation corresponds to a canonical transformation with the scaling factor $\sqrt{\gamma}$. Employing natural units ($\hbar = m^* = -e = 1$), measuring the energy in units of $\hbar\omega_0$, and choosing $\gamma = \omega_0^{-1}$, we introduce the HO-length as a length scale leading to the following working Hamiltonian:

$$H = \frac{1}{2}(\{p_x - y[B_h + B\cos(kx+\varphi)]\}^2 + p_y^2) + \frac{1}{4}(x^2 + y^2).$$

(8)

The reader should note that the above includes a rescaling of the field strength. For a typical quantum dot in GaAs with $\hbar\omega_0 = 3$ meV and $m^* = 0.067 m_e$, for example, where m_e is the bare electron mass, $B=1$ corresponds to a field strength of 1.736 T and one unit of length equals 19.4 nm. Whenever giving values in SI units, in the following, we will use these specific values of $\hbar\omega_0$ and m^*. Figure 3 illustrates the parabolic potential and its first few eigenstates in comparison with the periodic field for typical values of the wave number k. For $\varphi=0$, the magnetic field has a maximum at $x=0$. For a positive phase φ, the position of this maximum is shifted from the origin towards negative x-values. For $\varphi = \frac{\pi}{2}$, the magnetic field is zero at $x=0$.

The rotational symmetry of the quantum dot in a pure homogeneous field is broken by the presence of the spatially modulated field. Apart from the scaling relation, there are no continuous symmetries in this case. For $B_h = 0$, the Hamiltonian possesses the following discrete symmetries:

$$H(B, k, \varphi; x, y) = H(-B, k, \varphi; x, -y) = H(B, k, \varphi+\pi; x, -y)$$

$$= H(B, k, -\varphi; -x, -y) = H(B, k, \pi-\varphi; -x, y).$$

(9)

For special values of φ this implies that the parity or the x-parity are conserved. Obviously if φ is equal to zero or π then parity is a conserved quantity. If we vary only a single parameter then we encounter exclusively avoided crossings between levels, belonging to the same parity, whereas eigenstates with different parity can become degenerate.[53] For $\varphi = \pm\frac{\pi}{2}$, the x-parity is conserved. Again exact level crossings occur only for states with different x-parity. For other values of φ and $B \neq 0$, there is no conserved quantity. In these cases, e.g., the charge density within the quantum dot can be of arbitrary geometry.

III. BASIS SET AND COMPUTATIONAL METHOD

We use a basis set expansion method for the numerical solution of the time-independent Schrödinger equation. Given our complete orthonormal set of functions $\{\Phi_n | n \in \mathbb{N}\}$, the solutions can be expanded as $\widetilde{\Psi}_i = \sum_{n=1}^{\infty} c_n^{(i)} \Phi_n$. Within our variational approach a finite number of basis functions is chosen, limiting the numerical approximation of the exact eigenstates to a finite subspace: $\Psi_i = \sum_{n=1}^{N} c_n^{(i)} \Phi_n$. The linear variational principle is equivalent to solving an eigenvalue problem $\mathbf{H}\mathbf{c}^{(i)} = E_i \mathbf{c}^{(i)}$ with $\mathbf{c}^{(i)} = (c_1^{(i)}, \dots, c_N^{(i)})$ and $\mathbf{H} = (H_{kl})$ where $H_{kl} = \langle \Phi_k | H | \Phi_l \rangle$. Since the calculated eigenvalues E_i are upper bounds for the true eigenvalues $\widetilde{E}_i$, convergence can be checked by increasing the number of basis functions.

The choice of the basis functions is crucial for the effective and accurate solution of the problem. According to experience, it is useful to choose a basis, for which at least a part of the Hamilton matrix is diagonal. In our case this could be the Hamiltonian of the quantum dot with zero magnetic field (pure HO). However, it turns out that such a HO basis leads to very poor convergence properties in the case of large wave numbers k, i.e., small periods of the field. This can be repaired by simply introducing a corresponding scaling factor R in the direction of the periodic field only (see relevant discussion in Appendix A). Moreover, to include the case of the presence of an additional homogeneous magnetic field B_h, a complex phase, borrowed from the exact eigenfunctions of the dot in the homogeneous field [Eq. (8) for $B=0$] is taken into account. Our basis therefore reads

$$\Phi_{nm}(x, y) = A_{nm} H_n(\sqrt{c}Rx) H_m(\sqrt{c}y)$$

$$\times \exp\left(-\frac{cR^2x^2}{2} - \frac{cy^2}{2}\right) \exp(i\alpha xy), \quad (10)$$

where H_n are the Hermite polynomials and A_{nm} the corre-

sponding normalization constants. The solutions in the case of a pure homogeneous magnetic field ($B=0$ but $B_h \neq 0$) are finite linear combinations of the above functions, if the scaling factor is chosen $R=1$.[13] Note that $c = \frac{\sqrt{2+B_h^2}}{2}$ and $\alpha = \frac{B_h}{2}$. Our basis functions are eigenfunctions of $H_0 = \exp(i\alpha xy)H_{HO}\exp(-i\alpha xy)$, where H_{HO} is the Hamiltonian for the anisotropic HO. This yields

$$H_0 = \frac{p_x^2}{2} + \frac{p_y^2}{2} + \frac{B_h^2 + R^4(B_h^2 + 2)}{8}x^2$$
$$+ \frac{1 + B_h^2}{4}y^2 - \frac{B_h}{2}(yp_x + xp_y). \qquad (11)$$

The eigenvalues of H_0 are $E_{n,m}^0 = \frac{\sqrt{B_h^2+2}}{2}[R^2(n+\frac{1}{2}) + (m+\frac{1}{2})]$. Now we rewrite the total Hamiltonian $H = H_0 + H_1$ where

$$H_1 = \frac{1}{4}\left(1 - R^2 - \frac{B_h^2(1+R^2)}{2}\right)x^2 + \frac{B_h^2}{4}y^2 + \frac{B_h}{2}(xp_y - yp_x)$$
$$+ \frac{1}{2}\{[2B_hB\cos(kx+\varphi) + B^2\cos^2(kx+\varphi)]y^2$$
$$- ikB\sin(kx+\varphi)y - 2B\cos(kx+\varphi)yp_x\}. \qquad (12)$$

For the evaluation of the corresponding matrix elements of H_1, we refer the reader to Appendix B.

IV. RESULTS AND DISCUSSION

Our model system possesses three parameters: the amplitude B, the wave number k, and the phase φ of the magnetic field. First we will discuss the energy spectra depending on the field amplitude B and compare them with the spectrum of the quantum dot in a homogeneous field. Subsequently we will present spectra as a function of k showing different characteristics, depending on whether the wavelength is much larger, comparable to, or much smaller than the HO length of the quantum dot. Additionally, being close to experiment, we estimate electrochemical potentials with the constant interaction model. The magnetization of the system for zero temperature will also be investigated. Finally, we present probability and current densities for the ground state in some particular configurations. This provides us with a qualitative understanding of the evolution of the ground state with varying parameters.

A. Spectra with varying field amplitude

Before we discuss the behavior and properties in the presence of the periodic magnetic field, let us, for reasons of comparison, briefly summarize some basic facts for the case of a homogeneous field of strength B_h. The eigenenergies are given by $E_{n_1,n_2} = \hbar\omega_1(n_1+\frac{1}{2}) + \hbar\omega_2(n_2+\frac{1}{2})$ where the frequencies in natural units are given by $\omega_{1,2} = \frac{1}{\sqrt{2}}\sqrt{1 + B_h^2 \pm (B_h^4 + 2B_h^2)^{1/2}}$. For $B_h > 0$, ω_1 is a monotonically increasing and ω_2 is a monotonically decreasing function of B_h. The difference of both is the cyclotron frequency $\omega_1 - \omega_2 = |B_h| \hat{=} \frac{|eB_h|}{m} =: \omega_c$. Therefore the energies can be rewritten as
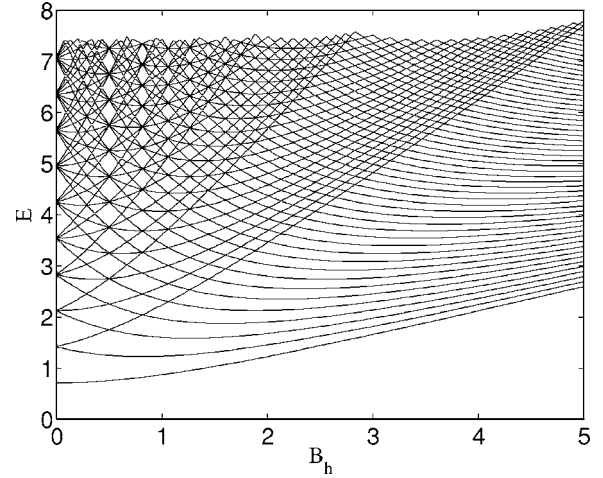

FIG. 4. The lowest 55 energies of the isotropic HO in a homogeneous magnetic field plotted as functions of B_h. Natural units are used.

$$E_{n_1,n_2} = \hbar\left[\omega_2(n_1 + n_2 + 1) + \omega_c\left(n_1 + \frac{1}{2}\right)\right]. \qquad (13)$$

In Fig. 4 the lowest 55 energy levels are plotted as a function of B_h. Without magnetic field, states with equal $n = n_1 + n_2$ are degenerate; the degree of degeneracy is $n+1$. When a weak magnetic field B_h is switched on, this degeneracy is lifted and the energy levels are split into groups. The group belonging to n has the total width $n\hbar\omega_c$. The higher the excitation, the larger the width of the level group at a given field strength. Therefore, for a given field strength, groups with sufficiently large n have to overlap. Since the magnetic quantum number is conserved, only exact level crossings occur. With increasing field strength, level degeneracies are encountered for the ratio $\omega_1 : \omega_2$ being a rational number. Pronounced energy gaps between degenerate groups of levels occur, if $\omega_1 : \omega_2$ is close to the ratio of small natural numbers, e.g., $\omega_1 : \omega_2 = 2$ corresponding to $B_h = 0.5$. For very large field strengths B_h, we have $\omega_c \gg \omega_2$. States with equal n_1 then belong to the same Landau band: the separation $\hbar\omega_c$ of the Landau bands is large and in between are accordingly many energy levels separated by $\hbar\omega_2$.

Let us now discuss the spectra of the quantum dot in a periodic magnetic field possessing the wave number $k=1$ as a function of the field amplitude. We begin with the case $\varphi = 0$ shown in Fig. 5(a). With increasing B the degenerate HO energy levels for $B=0$ split increasingly thereby forming groups. For small amplitudes, this splitting is proportional to B, and can be obtained by first order degenerate perturbation theory. In contrast to the case of the homogeneous field, the energy levels within one group are not equidistantly spaced and the total energetical width of one group is smaller for equal amplitudes. *This smaller splitting can be understood qualitatively by the fact that the unperturbed wave function sees a smaller spatial magnetic field average in case of a periodic field.* With increasing amplitude there are many avoided and exact level crossings. States being degenerate for $B=0$ possess the same parity. They can become exactly
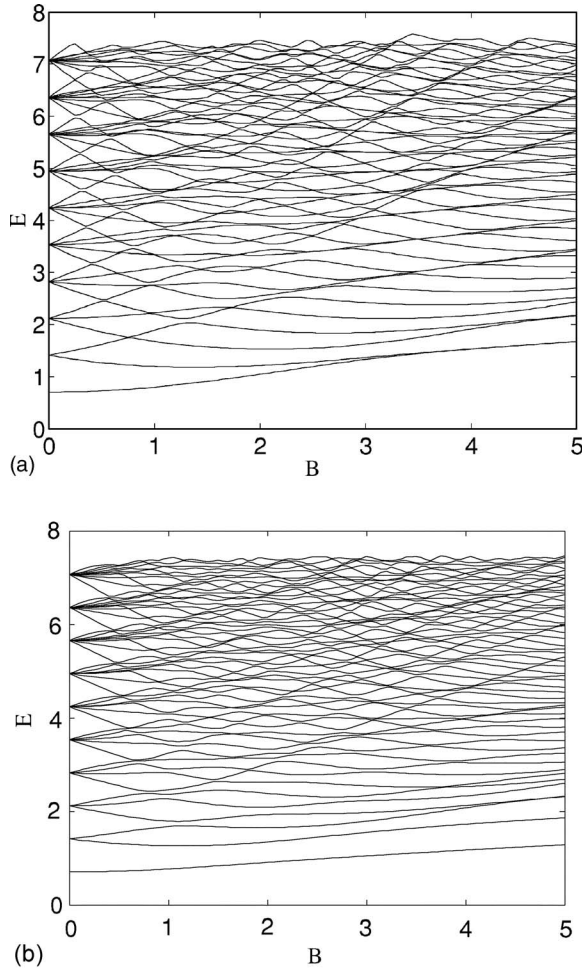
(a)

(b)

FIG. 5. Spectra with varying field amplitude for $k=1$ and the phases (a) $\varphi=0$ and (b) $\varphi=\frac{\pi}{4}$. Natural units are used.

degenerate with levels belonging to energetically neighboring groups, and will have avoided crossings with levels originating either from the same or from the next but one group. The grouping of exact degeneracies and resulting series of energy gaps, which occur for certain values of B_h in the homogeneous field case, cannot be observed in the presence of a periodic field. There are, however, individual energy gaps in the spectrum for certain values of B. To see this more clearly, we calculate the value $\Delta_2(n)=E_n-E_{n-1}$, where E_n is the energy of the nth excited state. Figure 6 illustrates Δ_2 for $k=1$, $\varphi=0$ for the amplitudes $B=0.2, 0.9$, and 1.2. For $B=0.2$ the positions of the peaks are the same as for the HO without field: $n=2,6,12,20,30,(42),\ldots$. The height of the peaks decreases with increasing n because the total splitting of one group is larger for higher n. This is equivalent to the statement that the level groups have to overlap for sufficiently high energies. For $B=0.9$ the peaks are at the positions $n=4, 8, 12, 20$, and 34 and for $B=1.2$ peaks are at $n=4, 12, 24$, and 34. Generally the height of the peaks decreases with increasing field strength. If the level dynamics is dominated by avoided crossings, the peak positions of Δ_2 can change rapidly with the system's parameters, thereby providing a coming and going of individual energy gaps. For large values of B we do not observe a structure in the spectrum
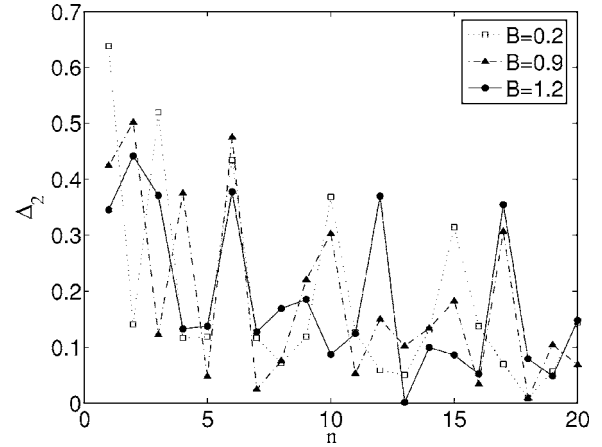

FIG. 6. Δ_2 for $k=1$ and $\phi=0$ for the three field amplitudes $B=0.2$, $B=0.9$, and $B=1.2$.

comparable to the Landau bands. The energy of the ground state is increasing with increasing field amplitude. However, *in contrast to the homogeneous field case the derivative $\frac{dE}{dB}$ is not monotonic.* For $B>3$ the ground state and the first excited state become nearly degenerate and for $B>4.5$ the second and third excited state are approximately degenerate as well, i.e., the corresponding levels group in pairs. We remark that an exact degeneracy of excited states, possessing different symmetry, is possible for $\varphi=0$. An intuitive explanation of this effect will be given in Sec. IV B after reconsidering the energy spectra as a function of the wave number. A manifestation of this effect on the probability density of the ground state will also be provided in Sec. IV E.

Let us now discuss the spectrum for $\varphi=\frac{\pi}{4}$ [Fig. 5(b)]. In this configuration we have only avoided level crossings. In the regime of field amplitudes considered here, the ground state does not become degenerate with the first excited state, but the second and third excited states have approximately the same energy for $B>4.5$. The increase of the ground state energy with increasing B is weaker compared to the case $\varphi=0$ but, at $B=5$ the energies of the first, second, and third excited states are higher in the case $\varphi=\frac{\pi}{4}$ compared to the ones of the case $\varphi=0$. Comparing the exact energies with perturbation theory shows again a good agreement, if the field amplitude is sufficiently small. The total energy splitting of a level group is in first order perturbation theory proportional to $B\cos(\varphi)$. Therefore the field-dependence of the splitting is weaker for the case $\varphi=\frac{\pi}{4}$ compared to the case $\varphi=0$. This can clearly be observed in the spectra of Fig. 5.

B. Spectra with varying period of the magnetic field

Here we discuss the dependence of the spectra on the wave number k for several values of B and φ. Due to the dimensionless scaling we introduced in Sec. II B, the value of k can be altered if we vary, e.g., ω_0. Experimentally this can be done if we change the gate voltage as, e.g., done in Ref. 4.

A general feature for all investigated configurations (B, φ) is the diminishing influence of the magnetic field with in-

creasing value of k: For $k \to \infty$, the energetically low-lying part of the spectrum approaches the spectrum of the pure HO. The reason for this limiting behavior becomes clear if we use another gauge for the vector potential namely $\vec{A}' = \left[0, \frac{B}{k} \sin(kx), 0\right]$. In this gauge the Hamiltonian reads

$$H' = \frac{1}{2}\left[p_x^2 + \left(p_y + \frac{B}{k}\sin(kx)\right)^2\right] + \frac{1}{4}(x^2 + y^2)$$

$$= \frac{1}{2}(p_x^2 + p_y^2) + \frac{1}{4}(x^2 + y^2) + 2\frac{B}{k}\sin(kx)p_y + \frac{B^2}{k^2}\sin^2(kx).$$

$$(14)$$

The last two terms provide only a small perturbation, if the value of $\frac{B}{k}$ is sufficiently small. In the limit $k \to \infty$, the Hamiltonian H' becomes that of the pure HO. With increasing k, the calculated eigenenergies and probability densities converge quickly to those of the HO while the magnitude of the probability current decreases not that fast. A physical interpretation of this convergence behavior, making use of analogies to a multiwell potential, will be provided below after investigating all relevant effects.

1. Low field amplitude

In Fig. 7 we illustrate the spectra of the quantum dot as a function of k in the range $0 \leqslant k \leqslant 2$ for the field-amplitude $B = 0.11$ and the three cases (a) $\varphi = 0$, (b) $\varphi = \frac{\pi}{4}$, and (c) $\varphi = \frac{\pi}{2}$. With respect to our example setup ($\hbar\omega_0 = 3$ meV and $m^* = 0.067m_e$) this equals the range 61 nm $\leqslant \lambda \leqslant \infty$ where λ is the corresponding wavelength of the periodic field and $B = 0.194$ T in SI units. For all values of k and this field amplitude the level splitting is small compared to $\hbar\omega_0$, therefore there are only few crossings for the levels we display. At $k = 0$ the energies are those of the HO in a homogeneous field of strength $B \cos(\varphi)$. With increasing k, the splitting of the levels decreases monotonically. States which are quasidegenerate for large k are in the following said to belong to the same group. The nth group consists of n states. For moderate wave numbers ($k \approx 1$), these groups are clearly distinguishable for the manifold of excited states shown in Fig. 7.

In the case $\varphi = 0$ [Fig. 7(a)], there are systematic nearly degenerate excited states at $k = 0$ (homogeneous field). The reason for this is that the two frequencies $\omega_{1,2}$ have a ratio close to 7:6. Accordingly the first levels having nearly the same energy are $E_{6,0}$ and $E_{0,7}$. For $\varphi = \frac{\pi}{4}$ [Fig. 7(b)], the picture is very similar. For the considered energies, the level splitting is so small that the neighboring level groups do not overlap. In the case $\varphi = \frac{\pi}{2}$ [Fig. 7(c)], the magnetic field vanishes for $k = 0$, thus the levels are exactly the HO levels. For $k > 0$ the level splitting is much less than for the other values of the phase, because in this case the leading terms for the energy splitting are proportional to B^2.

2. Strong field amplitudes

In Figs. 8(a)–8(c) the energy spectra as a function of the wave vector are shown for different phases and in particular for a large field amplitude $B = 1$. For $k < 2$ there occur both crossings and avoided crossings of energy levels. Generally,
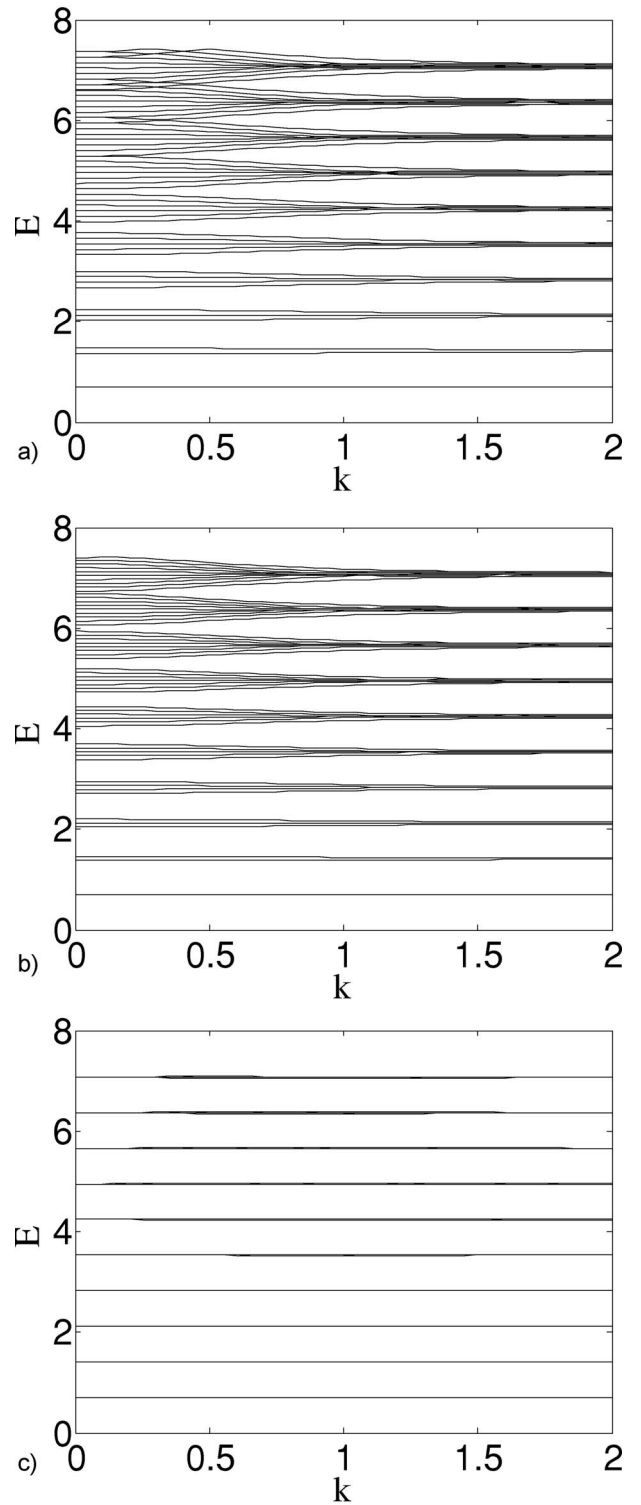

FIG. 7. Spectra as a function of the wave number k for $B = 0.11$ and (a) $\varphi = 0$, (b) $\varphi = \frac{\pi}{4}$, and (c) $\varphi = \frac{\pi}{2}$.

in this region of k, the level spacings are small, but there are values of k where the spectrum exhibits individual energy gaps.

The difference among the three cases $\varphi = 0$ [Fig. 8(a)], $\varphi = \frac{\pi}{4}$ [Fig. 8(b)], and $\varphi = \frac{\pi}{2}$ [Fig. 8(c)], due to different symmetry properties, can be seen clearly comparing the three
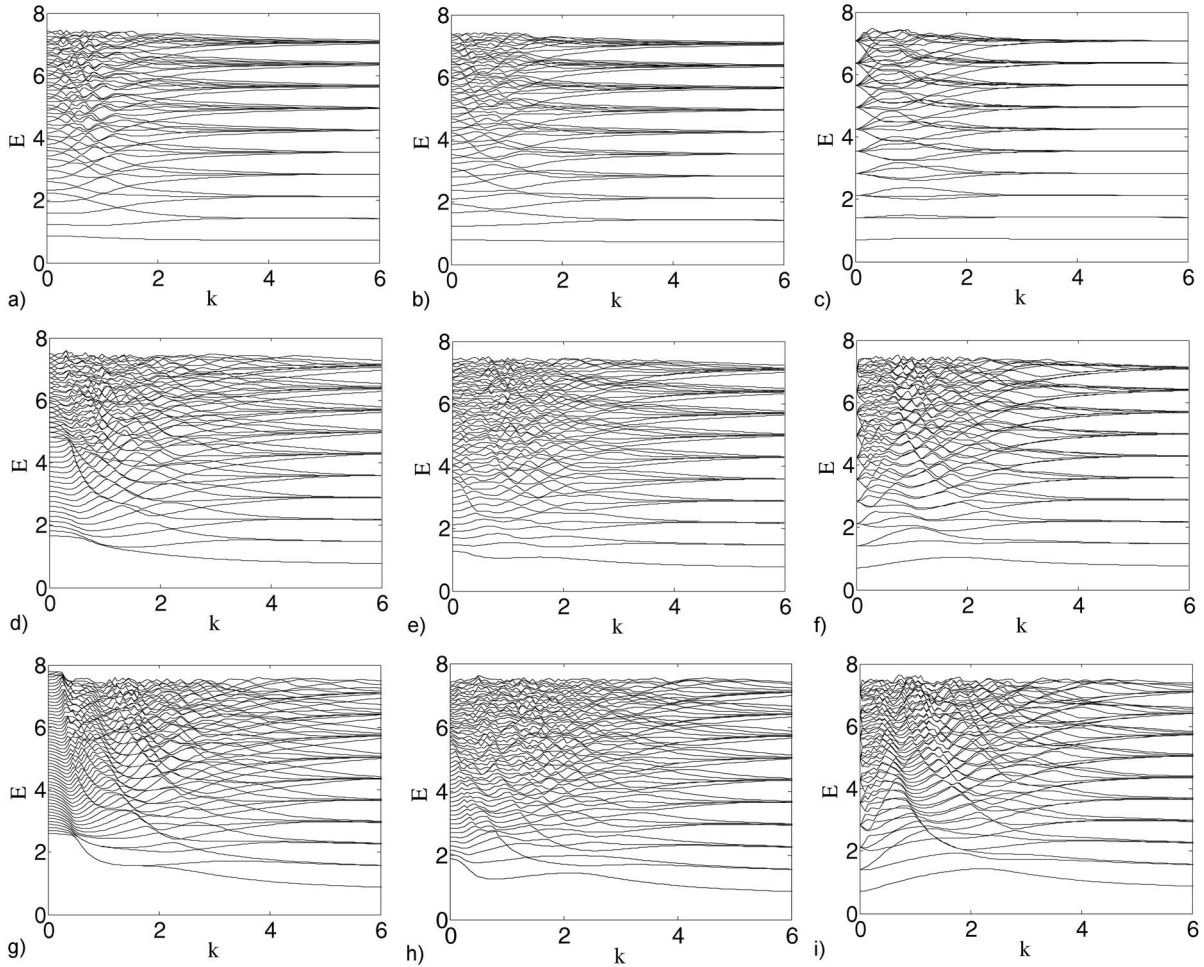
FIG. 8. Spectra as function of the wave number k for different values of the magnetic field amplitude B and the phase φ. The values of B are the same in each row: (a),(b),(c) $B=1$, (d),(e),(f) $B=3$, and (g),(h),(i) $B=5$ while the value of φ increases from left to right (a),(d),(g) $\varphi=0$, (b),(e),(h) $\varphi=\frac{\pi}{4}$, and (c),(f),(i) $\varphi=\frac{\pi}{2}$.

figures. For $\varphi=0$, there are exact degeneracies and we have more and larger gaps in the spectrum than for $\varphi=\frac{\pi}{4}$. Without parity conservation $\left(\varphi=\frac{\pi}{4}\right)$, all energy levels repel each other. For the phase $\varphi=\frac{\pi}{2}$, the levels tend to occur in pairs and there are again more gaps in the spectrum. This is because of the conserved x-parity, yielding no repulsion between two levels with different symmetry. For $k>2$ the level groups can be clearly distinguished. We observe that the mean energy spacing between two neighboring energy levels belonging to the same group of levels (that are degenerate for $B=0$) increases with increasing B and is roughly independent of the degree of excitation. However, the number of levels per group increases with increasing degree of excitation. Therefore the total width of the groups is larger for higher energy.

In Figs. 8(d)–8(f) the spectra for $B=3$ are illustrated. Three different regimes can be distinguished: Very small values, intermediate values, and large values of k. For very small k, the magnetic field is approximately homogeneous and at least for the lower part of the excitation spectrum the levels are approximately those of a homogeneous field case with an averaged magnetic field strength. For $\varphi=0$ [Fig. 8(d)], the energies of the lowest 12 levels decrease with in-

creasing k. In contrast to this, for $\varphi=\frac{\pi}{4}$ [Fig. 8(e)] the energy decreases for small values of k only for the lowest four levels. This has to be compared with the spectrum in a homogeneous field: In general, an infinitesimal increase of k equals to a lowering of the average field strength. In Fig. 4 we can see that for $B_h=3$, the energy of the lowest ten states decreases with slightly decreasing B_h. At $B_h=3\cos\left(\frac{\pi}{4}\right)\approx 2.1$, the energy of the lowest six states decreases if B_h is decreased slightly. For $\varphi=\frac{\pi}{2}$, we have the zero-field oscillator levels for $k=0$, which are split with increasing k. In contrast to the case of the presence of a homogeneous field, this splitting is not equidistant at all. For intermediate values of k, the spectrum has, similar to the case $B=1$, many avoided and exact level crossings. For $\varphi=0$ and $k\approx 1$, the ground state and the first excited state become nearly degenerate, which we observed already for the spectrum with varying field amplitude. Here we see that this feature occurs only for a small range of k-values, i.e., the levels split again for larger values of k. For other values of φ, this near-degeneracy does not occur. Again we can see the tendency of levels evolving in pairs for $\varphi=\frac{\pi}{2}$ [Fig. 8(f)]. Another feature of the spectra are "traces" of avoided crossings, which form patterns within the

main bodies of the spectra. These patterns are even more apparent for $B=5$.

Figures 8(g)–8(i) show the spectra for $B=5$. We observe also here that for sufficiently large values of k the calculated energy levels form nearly degenerate groups of levels. Comparison of the spectra for $B=1$, 3, and 5 at a fixed value of φ in the regime of sufficiently large k yields a splitting that increases with increasing field amplitude. In the case $B=5$ and $\varphi=0$ [Fig. 8(g)], the ground state and the first excited state are quasidegenerate for $0.5<k<2$. Furthermore the second and the third excited states are nearly degenerate for $0.5<k<1.5$. For $\varphi=\frac{\pi}{4}$ [Fig. 8(h)] and $\varphi=\frac{\pi}{2}$ [Fig. 8(i)] there are avoided crossings, but no quasidegeneracies of this kind. This can be understood qualitatively in the following way: It is energetically more favorable to shift the probability density towards regions with a small field strength. This statement is additionally validated by the evolution of the ground state probability density, presented in Sec. IV E. The expulsion of the electron from regions of large magnetic field strengths is expected to increase with increasing magnitude of the field gradient $\left|\frac{dB(x)}{dx}\right|=|Bk\sin(kx+\varphi)|$. It is therefore suggestive to compare our dot in the periodic field with the dot in the presence of a periodic potential of comparable size. The amplitude of this periodic potential has to increase with increasing B and the wavelength of this potential must decrease with increasing k. This results in an effective total potential, given by the periodic potential superimposed on the harmonic confinement of the dot, the features of which depend on B, k, and φ. For a fixed value of k and sufficiently small B, the total potential deviates only slightly from the harmonic confinement resulting in only one minimum of the total potential. If the value of B is large enough, the total potential will have several local minima, i.e., we encounter a multiwell potential. Only for the case $\varphi=0$, there are two global minima, with positions symmetric to the origin. Quasidegeneracies depend on the width and the depth of the wells. If the energy of the localized ground state in a single well is small compared to the energetical height of the barrier between the wells, the ground state becomes quasidegenerate with the first excited state. Depending on the barrier's height, we may also have quasidegenerate excited states. Our model allows us to explain the quasidegeneracies, observed in the spectra for varying B (Fig. 5). For $k=1$ and $\varphi=0$, the ground state is quasidegenerate for $B>3$ and the second and third excited states are quasidegenerate for $B>4.5$. For $\varphi=\frac{\pi}{4}$ the minima of the periodic potential are not anymore located symmetric to the origin and there are no quasidegeneracies. For a fixed, sufficiently large value of B, our total effective potential has the following dependence on k: If k is very small, the periodic potential changes slowly compared to the harmonic potential, thus the total potential has again only one minimum, i.e., we observe a nondegenerate ground state. When k is increased, the total potential develops several local minima. In the case $\varphi=0$, we obtain a quasidegenerate ground state. For $B=5$ [Fig. 8(g)] this happens at $k=0.5$ and we also have degenerate excited states in this case. The ground state energy is generally higher when the wells are narrower. Increasing k further makes the wells narrower. The energy of the quasidegenerate excited states increases com-

pared to the barrier's height, resulting in a gradual lifting of the quasidegeneracies in the spectrum. At $k=1.5$ the degeneracy of the second and third excited states is lifted again and accordingly for $k\approx2$ the degeneracy of the ground and first excited states is also lifted. For $\varphi=\frac{\pi}{2}$ [Fig. 8(i)] the minima of the absolute field strength are again located symmetrically around the origin, but the field is zero at $x=0$. Having worked out the similarities of a dot in a periodic magnetic field and a periodic potential one should keep in mind an important difference: In the first case, the ground state energy increases with increasing k, for large values of k, whereas in our system, the energy decreases with increasing k for sufficiently large values of k.

Finally let us comment on the relevance of the spin degrees of freedom in the case of a nonvanishing g-factor. The spin contribution to the Hamiltonian reads

$$H_{\text{spin}}=\frac{g\mu_B}{2}\vec{B}(x)\vec{\sigma}, \tag{15}$$

where σ_i are the Pauli matrices, g is the effective Landé g-factor, and μ_B the Bohr magneton. In the case $\vec{B}(x)=\hat{e}_zB\cos(kx+\varphi)$, there is no coupling between spin-up and spin-down states and the spin term is equivalent to an additional periodic potential $V_\pm(x)=\pm\frac{g\mu_B}{2}B\cos(xk+\varphi)$ for spin-up and spin-down states, respectively. Preliminary results for the spectrum including spin show that for a fixed value of the wave number and $\varphi=0$ spin-up states are lifted and spin-down states are lowered in energy compared to the spinless case. It is remarkable that the energetic splitting of the spin eigenstates depends on the degree of excitation and is not linearly increasing with increasing amplitude of the field. The reason for this is that the energy of the electron can be minimized by changing the probability density. A spin-up electron is pushed towards the maxima of the field strength and a spin-down electron is pushed towards the minima of the field strength, assuming $g<0$. For $\varphi=\frac{\pi}{2}$ there is no energy splitting of the spin eigenstates at all. In order to simulate a realistic situation, we have to take into account that the periodic magnetic field generated by magnetic stripes has two nonzero components, i.e., $\vec{B}(x)=\hat{e}_zB\cos(kx+\varphi)+\hat{e}_xB\sin(kx+\varphi)$. In this case there is a coupling between spin-up and spin-down states and we obtain avoided crossings whereas in the $\vec{B}(x)\|\hat{e}_z$ case we observe crossings of energy levels belonging to different spin. Several qualitative features of the spectra obtained without spin are not changed if the spin is taken into account. Those are among others the degeneracies for large values of k, the twofold degeneracies of the energetically lowest states for $k=1$, and large values of the field amplitude and the asymmetric splitting of energy levels for small field amplitudes. A complete discussion of the influence of the spin is, however, beyond the scope of this investigation.

C. Electrochemical potentials

For direct comparison with experimental results, we present the electrochemical potentials calculated in the simple constant interaction model. With this model, some

features of the spectra of few electron quantum dots in homogeneous magnetic fields have successfully been described.[4] The electrochemical potential for the n-electron quantum dot is given by $\Delta(n+1) = E_n + n\frac{e^2}{C}$, where E_n is the energy of the nth excited single electron state and C is the capacitance of the dot. Neglecting the spin dependent contributions in the Hamiltonian, each of the above calculated single electron states is twofold degenerate. This yields $\Delta(2n) - \Delta(2n+1) = \frac{e^2}{C}$ which is the constant charging energy. According to Ref. 4, we have chosen $\frac{e^2}{C} = \frac{1}{2} \approx \frac{\sqrt{2}}{3}\hbar\omega_0$. In Fig. 9(a), the electrochemical potentials for $k=1$ and $\varphi=0$ are provided as a function of B. The features of the spectrum [Fig. 5(a)] are reobtained. Avoided or exact level crossings give minima in the difference $\Delta(n+1) - \Delta(n)$. The (quasi-) degenerate groups of levels can be observed as groups of equidistantly spaced values of Δ. For example, for high values of B, the lowest four energy levels are quasidegenerate and the larger spacing between $\Delta(4)$ and $\Delta(5)$ is eye-catching. In Fig. 9(b), we show $\Delta(n)$ as a function of k for $B=5$ and $\varphi=0$. Again we can observe the different grouping of levels for different values of k. In Fig. 9(c), the electrochemical potentials as a function of the phase φ for $B=5$ and $k=1$ are provided. The quasidegeneracy of the ground and the first excited state, as well as that of the second and third excited state, respectively, occurring for $\varphi=0$, are lifted if the value of φ is increased. For $\varphi \approx 0.4$ there is an avoided crossing of the first and the second excited states, therefore, we observe a kink in the corresponding electrochemical potentials. For $\varphi \approx \frac{\pi}{4}$ we reobtain the avoided crossing of the second and third excited state. For $\varphi = \frac{\pi}{2}$, the spacing of the electrochemical potentials corresponding to the ground, the first excited, and the second exited states is relatively large.

D. Magnetization

Let us investigate the magnetization of our quantum dot for zero temperature. The magnetization M is given by $M = -\frac{dE}{dB_h}$ (Ref. 54) where E is the ground state energy. First we remark that the magnetization is zero for $\varphi = \frac{\pi}{2}$. This can be seen by using the Hellmann-Feynman theorem

$$\frac{dE_n}{dB_h} = \left\langle n \left| \frac{\partial H}{\partial B_h} \right| n \right\rangle. \tag{16}$$

The derivative of the Hamiltonian for $B_h = 0$ is

$$\left. \frac{\partial H}{\partial B_h} \right|_{B_h=0} = -2yp_x + 2By^2 \cos(kx + \varphi). \tag{17}$$

As discussed above, in the case $\varphi = \frac{\pi}{2}$, the Hamiltonian possesses an x-parity symmetry. Therefore the wave function Ψ is either an even or an odd function of x. Integrating

$$\left. \Psi^* \frac{\partial H}{\partial B_h} \Psi \right|_{\varphi=\pi/2} = -\Psi^* 2yp_x \Psi - \Psi^* 2By^2 \sin(kx)\Psi, \tag{18}$$

being an odd function of x, yields therefore zero.

Figure 10 shows in the upper panel contour plots of the magnetization as a function of B and k for the phases
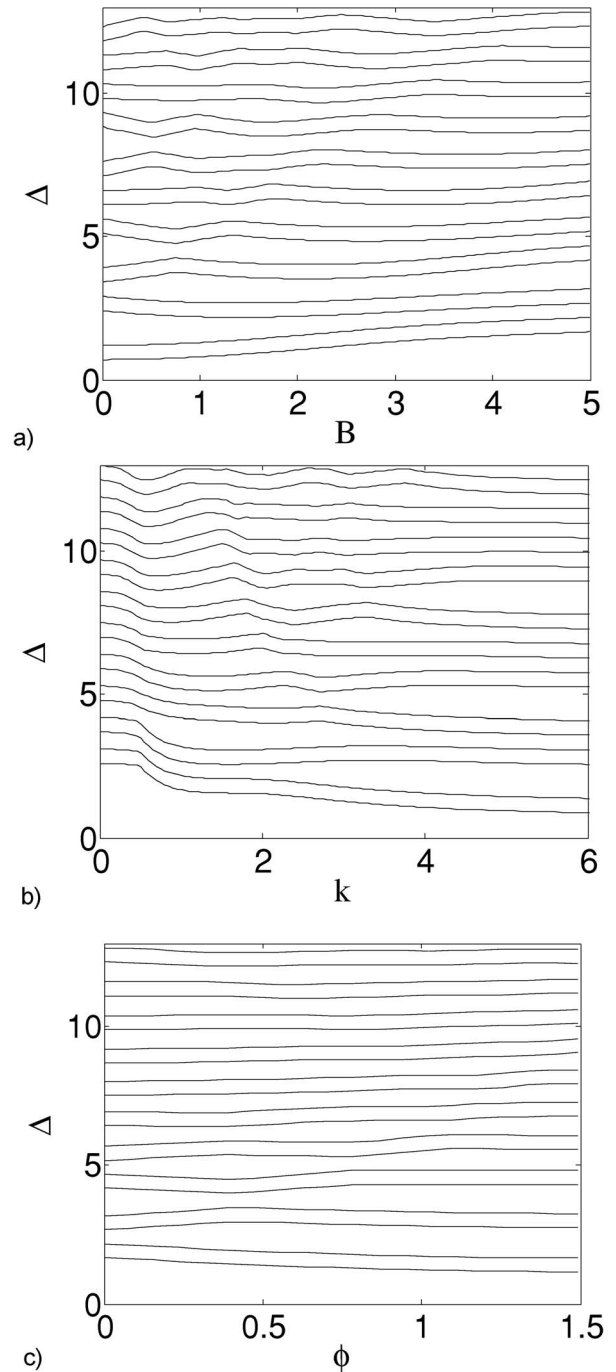

a)

b)

c)

FIG. 9. Electrochemical potentials (a) for $k=1$ and $\phi=0$ as a function of B, (b) for $B=5$ and $\phi=0$ as a function of k, and (c) for $B=5$ and $k=1$ as a function of φ.

(a) $\varphi=0$, (b) $\frac{\pi}{4}$, and (c) $\frac{\pi}{3}$. For a homogeneous field ($k=0$) with strength $B_h = B\cos(\varphi)$, the ground state possesses the energy $E_{00} = \frac{\sqrt{2 + B_h^2}}{2}$. Therefore the magnetization is given by

$$M = -\frac{B_h}{2\sqrt{2 + B_h^2}}. \tag{19}$$

The magnetization of the single electron quantum dot in a homogeneous magnetic field is zero for $B_h=0$ and decreases
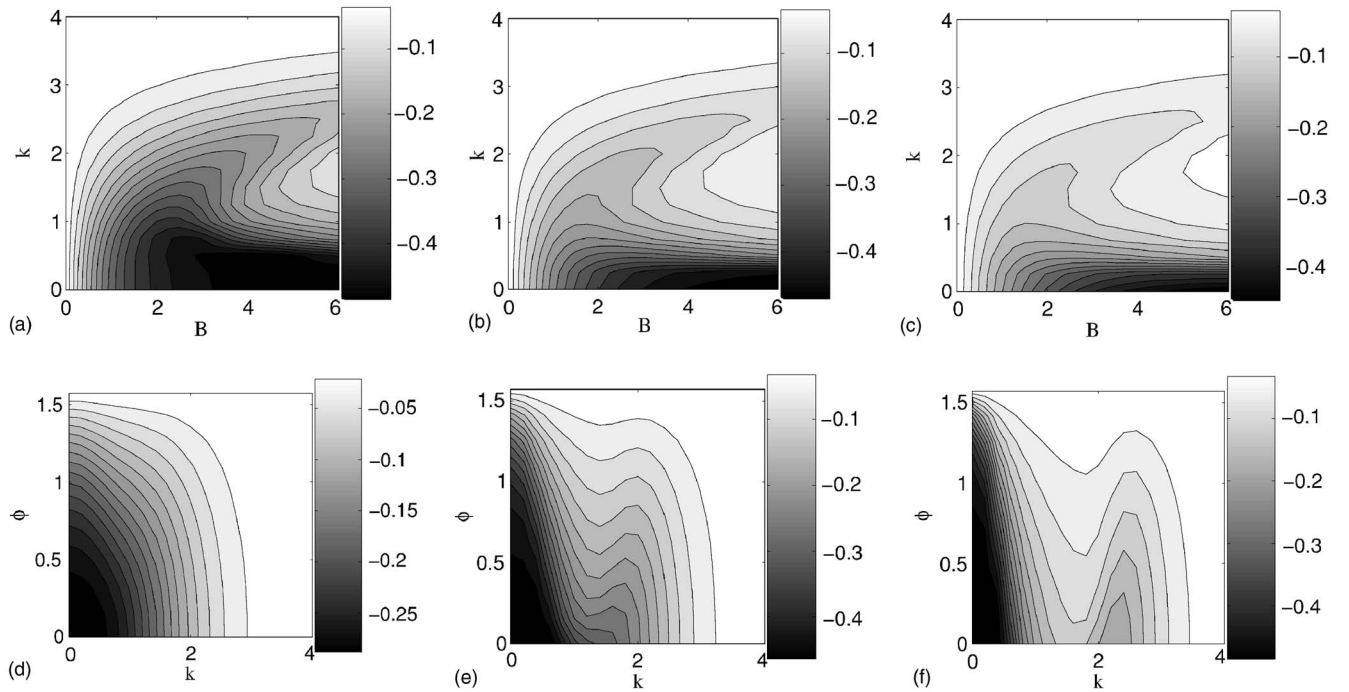
FIG. 10. Upper row: Contour plot of the magnetization as a function of B and k, for the three cases (a) $\varphi=0$, (b) $\varphi=\frac{\pi}{4}$, and (c) $\varphi=\frac{\pi}{3}$. Lower row: Magnetization as a function of k and φ. The field amplitude from left to right is (d) $B=1$, (e) $B=3$, and (f) $B=5$.

with increasing B_h. For $B_h \rightarrow \infty$, the magnetization goes to $-\frac{1}{2}$. Turning on a finite wave vector k let us follow the magnetization, e.g., along the line $k=1$. The magnetization is zero for $B=0$ and for small values of B decreases with increasing field strength. Subsequently M reaches a minimum and increases again for further increasing values of B. If we consider the magnetization for a larger value of k, the position of the minimum moves to larger values of B while the minimal value of M increases. For large values of k, the magnetization is very close to zero.

In the lower panel of Fig. 10 the dependence of the magnetization on k and φ is shown for the values $B=1$, 3, and 5. For $B=1$, the magnetization is minimal for $k=0$ (homogeneous field) and rises monotonically towards zero with increasing k. For larger amplitudes B, the magnetization develops a second minimum with varying k. The position of this local minimum moves to larger values of k with increasing B and the corresponding well-depth decreases. In all cases M goes to zero for $k \rightarrow \infty$.

E. Probability densities and probability current densities

To understand the evolution of the wave functions in a periodic magnetic field, let us study the corresponding probability densities and probability currents in the quantum dot. Instead of illustrating the density $\Psi^*\Psi$ we show the square root $|\Psi|$ of it, making it easier to see details in the case of a small density. The probability current density is defined by

$$\vec{j} = \frac{1}{2i}(\Psi^* \nabla \Psi - \Psi \nabla \Psi^*) + \vec{A}\Psi^*\Psi. \tag{20}$$

Figure 11 shows the densities and current densities for different field amplitudes $B=1$, 3, and 5 for $k=1$ and $\varphi=0$ for the ground state. With increasing field amplitude the charge is gradually shifted towards the regions where the magnitude of the magnetic field is small, while the region around $x=0$, being the position of the maximum of the field, is depleted. For $B=5$ [Fig. 11(c)], the charge density is split into two well-separated parts. The density for the first excited state possesses nearly the same distribution. We remind the reader that for these field parameters this effect is accompanied by an approximate energetical degeneracy of the ground and first excited state. The splitting of the probability density of the ground state is extremely sensitive to the phase φ of the magnetic field. Even very small deviations of φ from zero move the absolute field minima and lead to a ground state having almost all its probability shifted towards the nodal line of the field which is closer to the origin. The density of the first excited state is then localized at the opposite direction. This is in agreement with our comparative explanation of the spectra via a double well potential (see the corresponding discussion in Sec. IV B). If one well is slightly deeper, the ground state is localized in this deeper well and the first excited state in the second well. In all considered configurations the circulation of the current is counterclockwise, if the magnetic field is directed in the positive z-direction and clockwise for the magnetic field being directed in the negative z-direction. For $\varphi=0$ and as long as the ground state is not split, the current circulates around the origin, similar to the case of the presence of a homogeneous field. For $B=5$, there are two separate islands of currents: one on top of each half of the probability distribution. The current is smaller, compared to $B=3$, since the magnetic field seen by the electron is smaller.
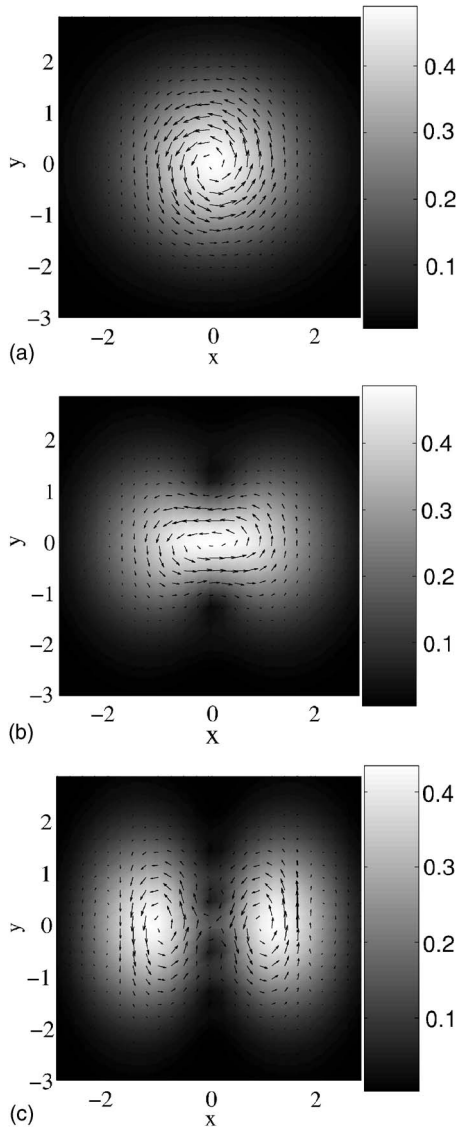
FIG. 11. Probability density $\sqrt{\Psi^*\Psi}$ and probability current densities of the ground state in the periodic field for $k=1$ and $\varphi=0$. The amplitude of the field is (a) $B=1$, (b) $B=3$, and (c) $B=5$. The splitting of the ground state is accompanied by the quasidegeneracy of the ground and the first excited states. Current density in arbitrary units.

Figure 12 shows a sequence of probability densities and currents for different values of k with $B=5$ and $\varphi=\frac{\pi}{4}$, respectively. First we consider the case of a homogeneous field, i.e., $k=0$ [Fig. 12(a)]. This field causes a compression of the charge density towards the origin and a counterclockwise flow of the current. The magnitude of the current is much larger compared to that in a periodic magnetic field. The following series of graphs is for the cases $k=1, 2, 2.5, 3$, and 4, respectively. The field strength possesses for general k a nodal line at $x=\frac{\pi}{4k}$. For $k=1$ [Fig. 12(b)] the width of the charge distribution is smaller in the x- than in the y-direction. The ground state wave function is shifted towards this absolute field minimum. Comparing a region with a positive

magnetic field component to a region with a negative one, the circulation of the current changes from counterclockwise to clockwise. For $k=2$ [Fig. 12(c)], the situation is similar. For $k\approx2$, the ground state energy reaches a local maximum and decreases subsequently with increasing k. For $k=2.5$ [Fig. 12(d)] we observe the charge density to move away from the area near the absolute magnetic field minimum. For $k=3$ [Fig. 12(e)] the current still maps the spatial dependence of the magnetic field. The density is already very close to that of the quantum dot without magnetic field, it appears not to be shifted towards the absolute field minimum. To measure this shift of the probability density, we calculate the center of density, i.e., the expectation value $\langle\vec{r}\rangle=\int\Psi^*\Psi\vec{r}d^2r$. In Fig. 13(a) we show the x-coordinate of the center of density for $B=5$ and $\phi=\frac{\pi}{4}$ depending on k. The solid curve indicates the x-position of the nodal line of the field being closest to the origin. For $1<k<2$ the center of density is close to the zero of the field. When k becomes larger than 2, the center of density is much closer to the origin than the nodal line of the field. This is in agreement with our multiwell potential picture, where the wells become steeper with increasing value of k. For $k=4$ [Fig. 12(f)] the situation is very similar. The probability density is nearly the same as in the pure HO, *but the wave function is not*. It has a spatially varying complex phase $\exp(i\theta)$, which gives together with the vector potential $\vec{A}=[-yB\cos(kx+\varphi),0,0]$ rise to the probability current density, which is smaller than for $k=3$ and changes its direction of circulation with each change of sign in the magnetic field. In terms of the phase θ, the current [Eq. (20)] reads $\vec{j}=\Psi^*\Psi(\vec{A}+\nabla\theta)$. It turns out that for large values of k, θ is approximately given by $\theta\approx\frac{yB}{k}\sin(kx)$. The x-components of both contributions, $\vec{A}$ and $\nabla\theta$, oscillate with $\cos(kx)$ and have a finite amplitude yB. However, the gradient of the phase and the vector potential cancel each other approximately. The y-component of the current density is, for our gauge, solely determined by the phase, yielding $j_y\approx\frac{B}{k}\sin(kx)$. Therefore we conclude that for large values of k the magnitude of the current decreases proportional to $\frac{1}{k}$. In Fig. 13(b) we have plotted the integral of the probability current density $\int|\vec{j}|dxdy$ in arbitrary units for $B=5$ and $\varphi=0$ as a function of k. The solid curve is proportional to $\frac{1}{k}$ and fitted to the data point for $k=12$. The magnetization of the dot converges faster towards zero with increasing k than the magnitude of the current. The reason for this is several current loops with clockwise and counterclockwise directed flows, whose contributions to the magnetization cancel approximately. Comparing the currents for different amplitudes of the field and $\varphi=0$ (Fig. 11), we can explain the local minimum and the increase of the magnetization with increasing field strength (see Sec. IV D). As long as the maximum of the charge density is located near the origin, the wave function will react on the strong magnetic field: similar to the case of a homogeneous field, the magnetization decreases with increasing field strength. When the probability distribution begins to split and "move" towards the zeroes of the magnetic field, the electron sees an effectively smaller mag-
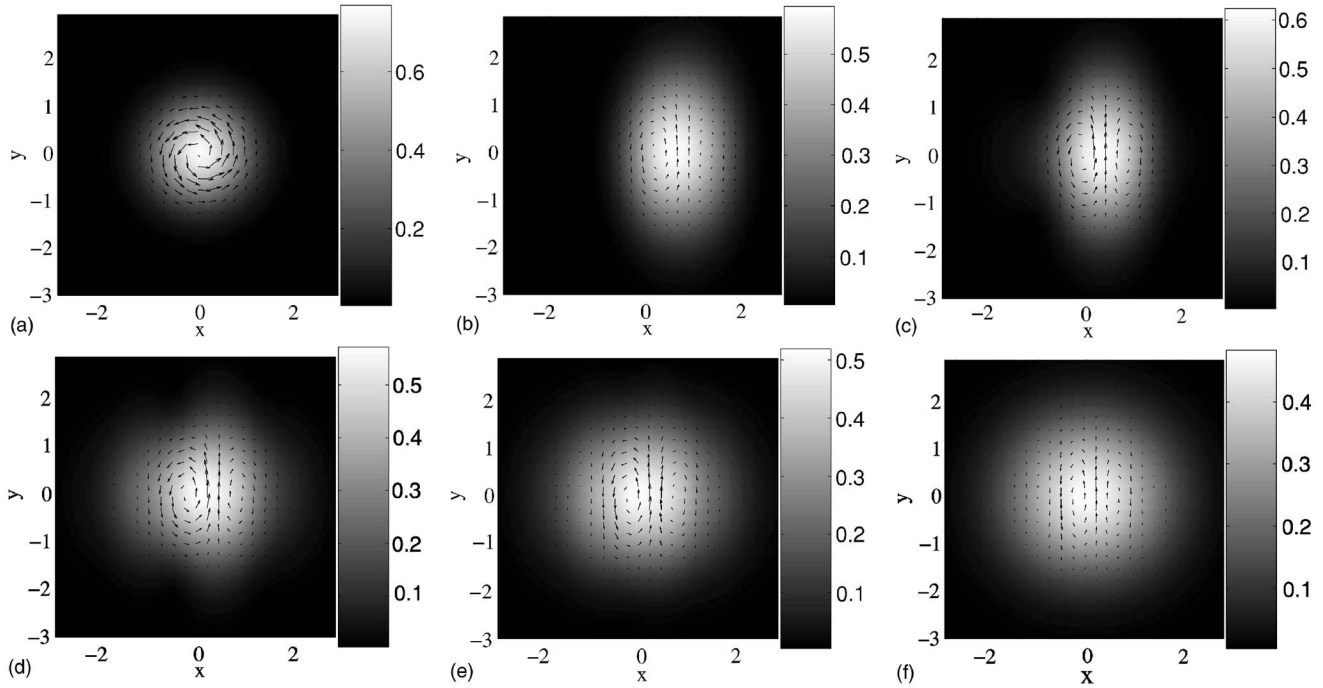
FIG. 12. Probability and current densities of the ground state in a magnetic field with amplitude $B=5$ and phase $\varphi=\frac{\pi}{4}$. The wave number is (a) $k=0$, (b) $k=1$, (c) $k=2$, (d) $k=2.5$, (e) $k=3$, and (f) $k=4$.

netic field, thereby decreasing the current and accordingly the absolute value of the magnetization.

V. SUMMARY

We have investigated the electronic structure of a single electron quantum dot exposed to a spatially periodic magnetic field. Our model quantum dot is described by a two-dimensional isotropic harmonic potential. Despite the simplicity of our model the spectrum of the quantum dot in a periodic field shows a rich dependence on the parameters of the field. It turns out that a periodic magnetic field possessing a wavelength significantly smaller than the characteristic length of the confining oscillator potential has almost no impact on the eigenvalues: In this case the lowest eigenenergies are approximately the same as in the pure HO. In the opposite case $k \to 0$ we encounter, of course, the well-known spectrum of the dot in a homogeneous magnetic field. For a sufficiently large field amplitude and in the intermediate regime of k-values, where the wavelength of the field is approximately the same as the HO length, the spectrum shows both avoided and, for special values of the phase of the field, exact level crossings.

The ground state of the quantum dot has been investigated in detail. In particular the magnetization for zero temperature and finite k shows a nonmonotonic behavior possessing a minimum with increasing B, in contrast to the case of a homogeneous field. We have further analyzed the probability and current densities as well, which lead us to an intuitive comprehension of the behavior of the dot. Many of the effects can be understood qualitatively via the picture of a periodic multiwell potential superimposed on the harmonic
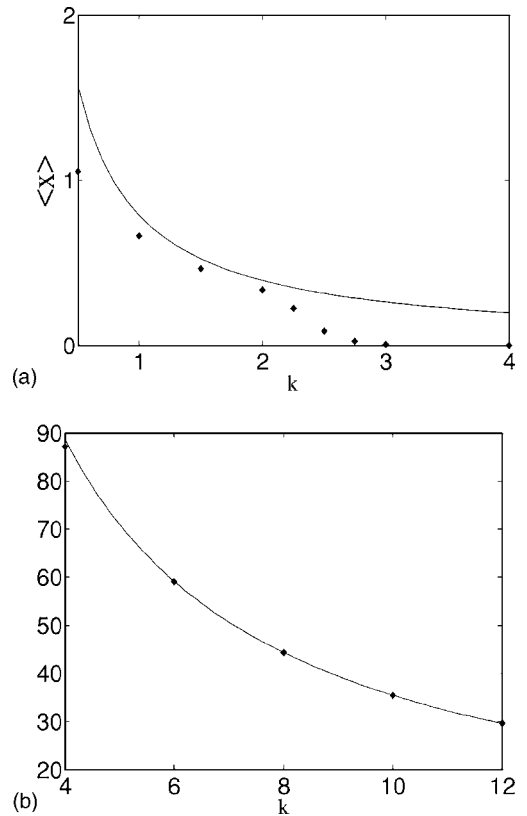

FIG. 13. (a) $\langle x \rangle$ as a function of k (diamonds) for $B=5$ and $\varphi = \frac{\pi}{4}$. The solid curve shows the x-position of the first nodal line of the magnetic field: $x = \frac{\pi}{4k}$. (b) Integral of the magnitude of the probability density current $\int |\vec{j}| dx dy$ as function of k, for $B=5$ and $\varphi = 0$ (diamonds). The solid curve is proportional to $\frac{1}{k}$, fitted to the data point at $k=12$. Arbitrary units for the current are chosen.
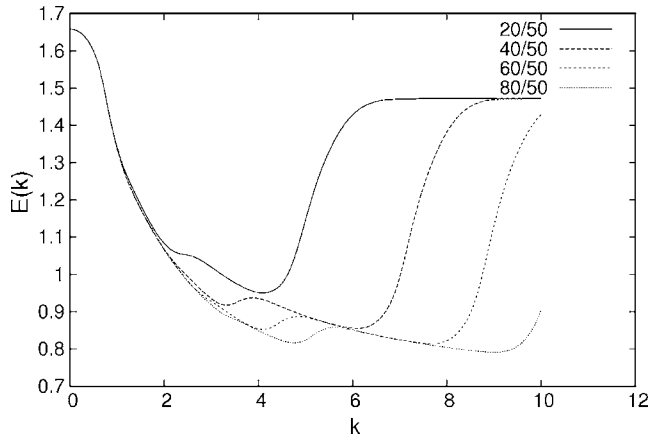
FIG. 14. Calculated ground state energy as a function of the wave number k for different numbers of basis functions Φ_{nm} with $R=1$ and $\alpha=0$. The basis is given by the relations $n<20$, 40, 60, and 80, respectively, and $m<50$.

FIG. 15. $S_{n,0}(\beta)$ for $n=1$, 5, 12, 25, 100, and 149. The numbers beneath the maxima are the corresponding values of n.

potential of the dot. If the wave number of the field is comparable to the oscillator length the probability density is pushed towards the nodal line of the field lying closest to the minimum of the confining potential. This behavior is highly sensitive to the phase φ. For large values of k the region with weak magnetic field becomes very narrow and pinning the electronic density is not anymore energetically favorable. Then the density of the ground state is almost the same as in the absence of the magnetic field. However, the imprinted current vanishes very slowly with increasing k. The direction of the probability current is thereby determined by the sign of the magnetic field. This explains why the magnetization of the dot is approximately zero for large k. The diverse profile of the probability density with respect to the parameters of the external field makes this system interesting for studies of electronic transport. Inclusion of the effects due to spin and/or investigating multielectron dots will be the subject of future investigations.

APPENDIX A: BASIS SETS WITH VARYING SCALING PARAMETER

Here we briefly discuss the importance of the scaling factor $R>1$, regarding the convergence of our numerical results. The pure HO basis set for $B_h=0$ and $R=1$ shows the following anomalous convergence behavior. For large values of the wave number k, there is a threshold behavior for the convergence with respect to the number of basis functions. Beginning with a small basis, the obtained eigenvalues are significantly higher than the correct eigenvalues. Increasing the size of the basis does not change the eigenvalues of the truncated Hamiltonian matrix until the number of basis functions reaches a critical value. Beyond this threshold the energy decreases rapidly with increasing number of basis functions until the lowest eigenvalues are converged. This is not what one could usually expect: doubling the number of basis functions might not change the eigenvalues and the calculation could be misinterpreted as being converged. In Fig. 14
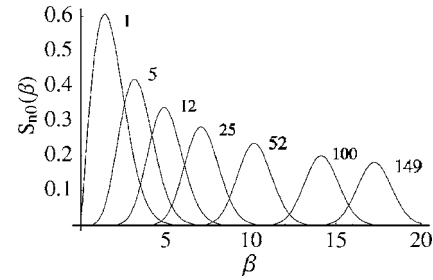
we show the calculated ground state energy as a function of the wave number k for different sizes of the basis set given in Eq. (10) with $R=1$ and $\alpha=0$. Here we have chosen $0 \leqslant m < 50$ and $0 \leqslant n < 20$, 40, 60, and 80 referring to the number of basis functions in the two Cartesian directions. Hence we have 1000, 2000, 3000, and 4000 basis functions, respectively. In all four cases the eigenvalue decreases with increasing k. Above some value of k, which depends on the basis size, the eigenvalue increases again, reaching a plateau. This increase is obviously nonphysical but, e.g., for $k=10$ the lowest eigenvalue remains the same for 1000 and 2000 basis functions. This unusual convergence behavior is due to the properties of the integrals $S_{n,i}\left(\frac{k}{Rc}\right)$ occurring in the matrix elements due to the periodic field (see Appendix B). They possess strongly localized peaks for large values of the dimensionless parameter $\beta=\frac{k}{Rc}$, if the difference of the indices $n-i$ is large. Figure 15 shows the graphs of $S_{n,0}(\beta)$ for several values of n. The position of the extrema is $\beta=\sqrt{2n}$ and the height is approximately proportional to $n^{-1/4}$. The larger the value of n is, the larger is the value of β, where $S_{n,0}(\beta)$ reaches its extremum. The extremum of the integral decreases relatively slowly with increasing n. Therefore, far off-diagonal matrix elements become important if the value of β is large and very large basis sets, such that all relevant matrix elements are part of the truncated Hamilton matrix, have to be used. Using a value of $R>1$ we can achieve that the value of β at the position of the extremum becomes smaller. On the other hand the HO eigenfunctions are approximated badly by the basis, if R is too large. Hence for a given k and size of the basis the calculated eigenenergies show a minimum with respect to R. By exploiting this variational property for the considered eigenvalues, we can choose a proper R for our investigations.

APPENDIX B: MATRIX ELEMENTS OF THE HAMILTONIAN

Here we present the matrix elements of the Hamiltonian in Eq. (7) with respect to the basis functions given in Eq. (10). Calculating the action of the operators x, y, ∂_x, and ∂_y on the basis functions is straightforward, using the recursion relations for the Hermite polynomials. For the calculation of the matrix elements of the periodic magnetic field, the integrals

$$\langle\Phi_{nm}|\cos(kx)|\Phi_{jl}\rangle = \frac{1}{\sqrt{\pi 2^{n+j}n!j!}}\int_{-\infty}^{\infty}e^{-a^2}H_n(a)H_j(a)\cos(\beta a)da$$

$$= \begin{cases} 0 & \text{for odd } n+j \\ S_{j,n}(\beta) := (-1)^{(j-n)/2}\sqrt{2^{n-j}\frac{n!}{j!}}\beta^{j-n}L_n^{j-n}\left(\frac{\beta^2}{2}\right)e^{-\beta^2/4} & \text{else} \end{cases} \qquad (B1)$$

$$\langle\Phi_{nm}|\sin(kx)|\Phi_{jl}\rangle = \frac{1}{\sqrt{\pi 2^{n+j}n!j!}}\int_{-\infty}^{\infty}e^{-a^2}H_n(a)H_j(a)\sin(\beta a)da$$

$$= \begin{cases} 0 & \text{for even } n+j \\ S_{j,n}(\beta) := (-1)^{(j-n-1)/2}\sqrt{2^{n-j}\frac{n!}{j!}}\beta^{j-n}L_n^{j-n}\left(\frac{\beta^2}{2}\right)e^{-\beta^2/4} & \text{else} \end{cases} \qquad (B2)$$

are needed. Here we imposed the dimensionless parameter $\beta := \frac{k}{R\sqrt{c}}$. L_n^{j-n} are associated Laguerre polynomials. This formula defines the $S_{j,n}$ only for $j \geq n$. Because of the obvious symmetry of the integrals with respect to the indices j and n, we define $S_{j,n} := S_{n,j}$ for $j < n$. To calculate $S_{n,j}$, we use the following recursion relations

$$S_{0,0}(\beta) = e^{-\beta^2/4}, \qquad (B3)$$

$$S_{n,0}(\beta) = (-1)^{n+1}\frac{\beta}{\sqrt{2n}}S_{n-1,0}, \qquad (B4)$$

$$S_{n,1}(\beta) = \left(\sqrt{n} - \frac{\beta^2}{2\sqrt{n}}\right)S_{n-1,0}, \qquad (B5)$$

$$S_{n,j}(\beta) = \frac{j+n-1-\frac{\beta^2}{2}}{\sqrt{nj}}S_{n-1,j-1} - \frac{\sqrt{(n-1)(j-1)}}{\sqrt{nj}}S_{n-2,j-2}. \qquad (B6)$$

With these formulas the calculation of the matrix elements is straightforward:

$$\langle\Phi_{n,m}|\cos^2(kx+\varphi)y^2|\Phi_{j,l}\rangle = \langle\Phi_{n,m}|\frac{1}{2}[1+\cos(2kx$$
$$+2\varphi)]y^2|\Phi_{j,l}\rangle$$
$$= \frac{1}{4c}\left(\delta_{n,j} + S_{n,j}(2\beta)\begin{cases}\cos(2\varphi) & \text{for even } n+j \\ -\sin(2\varphi) & \text{for odd } n+j\end{cases}\right) \times ((2l$$
$$+1)\delta_{m,l} + \sqrt{m(m-1)}\delta_{m,l+2} + \sqrt{l(l-1)}\delta_{m,l-2}), \qquad (B7)$$

$$\langle\Phi_{n,m}|\cos(kx+\varphi)y^2|\Phi_{j,l}\rangle = \frac{1}{2c}S_{n,j}(\beta)$$
$$\times\begin{cases}\cos(\varphi) & \text{for even } n+j \\ -\sin(\varphi) & \text{for odd } n+j\end{cases} \times ((2l+1)\delta_{m,l}$$
$$+ \sqrt{m(m-1)}\delta_{m,l+2} + \sqrt{l(l-1)}\delta_{m,l-2}), \qquad (B8)$$

$$\langle\Phi_{n,m}|\sin(kx+\varphi)y|\Phi_{j,l}\rangle = -\frac{1}{\sqrt{2c}}(\sqrt{m}\delta_{m,l+1} + \sqrt{l}\delta_{m,l-1})S_{n,j}(\beta)$$
$$\times\begin{cases}\sin(\varphi) & \text{for even } n+j \\ \cos(\varphi) & \text{for odd } n+j\end{cases}, \qquad (B9)$$

$$\langle\Phi_{n,m}|\cos(kx+\varphi)y\partial_x|\Phi_{j,l}\rangle = \frac{i\alpha}{2c}S_{n,j}(\beta)$$
$$\times\begin{cases}\cos(\varphi) & \text{for even } n+j \\ -\sin(\varphi) & \text{for odd } n+j\end{cases}[(2l+1)\delta_{m,l}$$
$$+ \sqrt{m(m-1)}\delta_{m,l+2} + \sqrt{l(l-1)}\delta_{m,l-2}] + \frac{R}{2}(\sqrt{j}S_{n,j-1}(\beta)$$
$$- \sqrt{j+1}S_{n,j+1}(\beta))\begin{cases}-\sin(\varphi) & \text{for even } n+j \\ \cos(\varphi) & \text{for odd } n+j\end{cases}$$
$$\times (\sqrt{l}\delta_{m,l-1} + \sqrt{l+1}\delta_{m,l+1}). \qquad (B10)$$

[1] L. L. Chang, L. Esaki, and R. Tsu, Appl. Phys. Lett. **24**, 593 (1974).

[2] R. Dingle, W. Wiegmann, and C. H. Henry, Phys. Rev. Lett. **33**, 827 (1974).

[3] P. M. Petroff, A. C. Gossard, R. A. Logan, and W. Wiegmann, Appl. Phys. Lett. **41**, 635 (1982).

[4] L. P. Kouwenhoven, D. G. Austing, and S. Tarucha, Rep. Prog. Phys. **64**, 701 (2001).

[5] J. Weis, R. J. Haug, K. von Klitzing, and K. Ploog, Semicond. Sci. Technol. **9**, 1890 (1994).

[6] L. Jacak, P. Hawrylak, and A. Wojs, *Quantum Dots* (Springer-Verlag, Berlin, 1998).

[7] S. M. Reimann and M. Manninen, Rev. Mod. Phys. **74**, 1283 (2002).

[8] K. v. Klitzing, G. Dorda, and M. Pepper, Phys. Rev. Lett. **45**, 494 (1980).

[9] D. C. Tsui, H. L. Störmer, and A. C. Gossard, Phys. Rev. Lett. **48**, 1559 (1982).

[10] C. W. J. Beenakker and H. van Houten, Solid State Phys. **44**, 1 (1991).

[11] V. Fock, Z. Phys. **47**, 446 (1928).

[12] C. G. Darwin, Proc. Cambridge Philos. Soc. **27**, 86 (1930).

[13] O. Dippel, P. Schmelcher, and L. S. Cederbaum, Phys. Rev. A **49**, 4415 (1994).

[14] M. Taut, J. Phys. A **27**, 1045 (1994).

[15] S. B. Trickey and W. Zhu, Phys. Rev. A **72**, 022501 (2005).

[16] P. S. Drouvelis, P. Schmelcher, and F. K. Diakonos, Europhys. Lett. **64**, 232 (2003).

[17] P. S. Drouvelis, P. Schmelcher, and F. K. Diakonos, Phys. Rev. B **69**, 155312 (2004).

[18] P. S. Drouvelis, P. Schmelcher, and F. K. Diakonos, J. Phys.: Condens. Matter **16**, 3633 (2004).

[19] H. W. Jiang and E. Yablonovitch, Phys. Rev. B **64**, 041307(R) (2001).

[20] G. Salis, Y. Kato, K. Ensslin, D. Driscoll, A. Gossard, and D. Awschalom, Nature (London) **414**, 619 (2001).

[21] F. M. Peeters and A. Matulis, Phys. Rev. B **48**, 15166 (1993).

[22] M. Calvo, Phys. Rev. B **48**, 2365 (1993).

[23] A. Matulis, F. M. Peeters, and P. Vasilopoulos, Phys. Rev. Lett. **72**, 1518 (1994).

[24] J. E. Müller, Phys. Rev. Lett. **68**, 385 (1992).

[25] H.-S. Sim, K. H. Ahn, K. J. Chang, G. Ihm, N. Kim, and S. J. Lee, Phys. Rev. Lett. **80**, 1501 (1998).

[26] B.-Y. Gu, W.-D. Sheng, X.-H. Wang, and J. Wang, Phys. Rev. B **56**, 13434 (1997).

[27] S. M. Badalyan and F. M. Peeters, Phys. Rev. B **64**, 155303

[28] (2001).

[28] H.-S. Sim, K. J. Chang, N. Kim, and G. Ihm, Phys. Rev. B **63**, 125329 (2001).

[29] A. Nogaret, S. J. Bending, B. L. Gallagher, and M. Henini, Phys. Rev. Lett. **84**, 2231 (1997).

[30] M. Hara, A. Endo, S. Katsumoto, and Y. Iye, Phys. Rev. B **69**, 153304 (2004).

[31] P. D. Ye, D. Weiss, R. Gerhardts, K. von Klitzing, K. Eberl, H. Nickel, and C. Foxon, Semicond. Sci. Technol. **10**, 715 (1995).

[32] P. D. Ye, D. Weiss, R. R. Gerhardts, M. Seeger, K. von Klitzing, K. Eberl, and H. Nickel, Phys. Rev. Lett. **74**, 3013 (1995).

[33] P. D. Ye, D. Weiss, R. R. Gerhardts, K. von Klitzing, K. Eberl, and H. Nickel, Surf. Sci. **361/362**, 337 (1996).

[34] A. Nogaret, S. Carlton, B. L. Gallagher, P. C. Main, M. Henini, R. Wirtz, R. Newbury, M. A. Howson, and S. P. Beaumont, Phys. Rev. B **55**, R16037 (1997).

[35] P. D. Ye, D. Weiss, R. Gerhardts, K. von Klitzing, and S. Tarucha, Physica B **249-251**, 330 (1998).

[36] R. R. Gerhardts, Phys. Rev. B **53**, 11064 (1996).

[37] D. P. Xue and G. Xiao, Phys. Rev. B **45**, 5986 (1992).

[38] R. Yagi and Y. Iye, J. Phys. Soc. Jpn. **62**, 1279 (1993).

[39] F. M. Peeters and P. Vasilopoulos, Phys. Rev. B **47**, 1466 (1993).

[40] G. Gumbs and C. Zhang, Solid State Commun. **115**, 163 (2000).

[41] M. Kato, A. Endo, S. Katsumoto, and Y. Iye, Phys. Rev. B **58**, 4876 (1998).

[42] M. Kato, A. Endo, M. Sakairi, S. Katsumoto, and Y. Iye, J. Phys. Soc. Jpn. **68**, 1492 (1999).

[43] M. Kato, M. Sakairi, A. Endo, S. Katsumoto, and Y. Iye, Physica E (Amsterdam) **6**, 735 (2000).

[44] T. Sasaki and H. Fukuyama, J. Phys. Soc. Jpn. **71**, 1108 (2002).

[45] P. D. Ye, D. Weiss, R. Gerhardts, G. Ltjering, K. von Klitzing, and H. Nickel, Semicond. Sci. Technol. **11**, 1613 (1996).

[46] A. Y. Rom, S. Fishman, R. Kosloff, and T. Maniv, Phys. Rev. B **54**, 9819 (1996).

[47] P. Schmelcher and D. L. Shepelyansky, Phys. Rev. B **49**, 7418 (1994).

[48] J. Yoshida, T. Ohtsuki, and Y. Ono, J. Phys. Soc. Jpn. **67**, 3886 (1998).

[49] R. Hennig and M. Suhrke, Phys. Rev. B **60**, 11535 (1999).

[50] Z.-L. Ji and D. W. L. Sprung, Semicond. Sci. Technol. **12**, 529 (1997).

[51] Z.-L. Ji and D. W. L. Sprung, Phys. Rev. B **56**, 1045 (1997).

[52] M. Przybylski, S. Chakraborty, and J. Kirschner, J. Magn. Magn. Mater. **234**, 505 (2001).

[53] J. von Neumann and E. Wigner, Phys. Z. **30**, 467 (1929).

[54] P. A. Maksym and T. Chakraborty, Phys. Rev. B **45**, 1947 (1992).